

# Efficient basis expansion for describing linear and nonlinear electron dynamics in crystalline solids

Shunsuke A. Sato<sup>1</sup> and Kazuhiro Yabana<sup>1,2</sup>

<sup>1</sup>*Graduate School of Pure and Applied Sciences,*

*University of Tsukuba, Tsukuba 305-8571, Japan*

<sup>2</sup>*Center for Computational Sciences, University of Tsukuba, Tsukuba 305-8577, Japan*

## Abstract

We propose an efficient basis expansion for electron orbitals to describe real-time electron dynamics in crystalline solids. Although a conventional grid representation in the three-dimensional Cartesian coordinates works robustly, it requires a large amount of computational resources. To reduce computational costs, we consider an expansion using basis functions with a truncation. A simple choice employing eigenstates of the ground state Hamiltonian with a truncation turned out to be useless. We have found that adding occupied eigenstates of nearby  $k$ -points to the truncated basis functions composed of eigenstates of the original  $k$ -point is crucially important. We demonstrate the usefulness of the method for linear and nonlinear electron dynamics calculations in crystalline SiO<sub>2</sub>.

## I. INTRODUCTION

In current frontiers of optical sciences, interactions of intense and/or ultrashort laser pulses with crystalline solids have been attracting substantial interests from both fundamental and technological points of view [1–8]. To describe interactions of visible or infrared laser pulses with crystalline solids, it is necessary to calculate time evolution of electron orbitals in a unit cell of solids under a time-varying, spatially-uniform electric field.

In the first-principles level, calculations based on the time-dependent density functional theory (TDDFT) [9] have been carried out. We have been developing a computational method solving the time-dependent Kohn-Sham (TDKS) equation in real time in a unit cell of solids in which a uniform grid representation in the three-dimensional Cartesian coordinates is used to express orbital wave functions [10–14]. A similar computational approach has also been developed and utilized in Ref.[15–18]. A computational method employing plane wave basis has also been developed [19]. These computational schemes are applicable to electron dynamics in linear regimes [10, 19] and nonlinear electron dynamics under intense laser pulses [11–17]. There are also a number of works solving the time-dependent Schrödinger equation in empirical periodic potentials [20–23].

Although numerical methods employing a uniform grid representation in the three-dimensional Cartesian coordinates works stably and robustly, time evolution calculations in this representation are computationally demanding. In particular, the required computational resource is excessively large when we couple the electron dynamics with the dynamics of macroscopic electromagnetic fields [24, 25]. We are thus urged to find a more efficient representation in which computational costs are reduced without harming numerical accuracy. In molecules and nano-sized materials, orbital expansions are often utilized for real time evolution calculations. For example in Ref.[26], time evolution calculations are achieved in a dense matrix representation employing truncated eigenfunctions of the static Kohn-Sham Hamiltonian with spatial-domain decompositions.

As basis functions in crystalline solids, one may suppose that a finite number of eigenstates of the static Kohn-Sham Hamiltonian at each  $k$ -point would serve as a natural choice. However, as will be shown, this truncation scheme does not work well. We will show that it is crucially important to use basis functions in which occupied eigenstates of nearby  $k$ -points are added to the eigenstates of the original  $k$ -point. We will illustrate usefulness

of the method in the time evolution calculation taking a system of SiO<sub>2</sub> described with a time-independent periodic potential.

The construction of the paper is as follows. In Sec. II, we describe theoretical frameworks and our proposal for the efficient basis functions. In Sec. III, we examine usefulness of the proposed basis expansion for linear response problems. In Sec. IV, applications to electron dynamics under pulsed electric fields is discussed. In Sec. V, we discuss computational aspects of the proposed method. In Sec. VI, a summary will be presented.

## II. BASIS FUNCTIONS FOR ELECTRON DYNAMICS CALCULATIONS

### A. Time-dependent Schrödinger equation

We consider electron dynamics in a crystalline solid under an optical electric field of visible or infrared frequencies. We assume a long wavelength limit: The wave length of the optical electric field is much longer than the length scale of the electron dynamics induced by the field. We treat the optical electric field in a unit cell as a time dependent, spatially-uniform electric field.

We consider the following time dependent Schrödinger equation for the Bloch orbitals to describe electron dynamics,

$$i\hbar \frac{\partial}{\partial t} u_{n\vec{k}}(\vec{r}, t) = h \left[ \vec{k} + \frac{e}{\hbar c} \vec{A}(t) \right] u_{n\vec{k}}(\vec{r}, t), \quad (1)$$

where  $u_{n\vec{k}}(\vec{r}, t)$  is a time dependent Bloch orbital which is periodic in space,  $u_{n\vec{k}}(\vec{r} + \vec{a}) = u_{n\vec{k}}(\vec{r})$ , where  $\vec{a}$  is a lattice vector. The Hamiltonian  $h[\vec{k} + e\vec{A}(t)/\hbar c]$  is assumed to have the following form:

$$h \left[ \vec{k} + \frac{e}{\hbar c} \vec{A}(t) \right] = \frac{1}{2m} \left( \vec{p} + \hbar \vec{k} + \frac{e}{c} \vec{A}(t) \right)^2 + V(\vec{r}) \quad (2)$$

where  $\hbar \vec{k}$  is a crystalline momentum.  $\vec{A}(t)$  is a time dependent, spatially-uniform vector potential. It is related to the optical electric field  $\vec{E}(t)$  by  $\vec{E}(t) = -\frac{1}{c} \frac{\partial}{\partial t} \vec{A}(t)$ .  $V(\vec{r})$  is an effective single-electron potential which is periodic in space. It may be nonlocal in space to include, for example, a norm-conserving pseudopotential and/or an exchange potential. When we describe the many-electron dynamics by the time-dependent Hartree-Fock or the TDDFT, we need to allow the potential  $V(\vec{r})$  to be time dependent.

## B. Choices of basis functions

To calculate the electron dynamics in practice, we need to express Eq. (1) in a matrix form. In the real-space grid representation, we discretize the equation using uniform grids in the three-dimensional (3D) Cartesian coordinates and express the Hamiltonian of Eq. (2) as a sparse Hermitian matrix [10]. We call it the 3D grid representation hereafter. Though this representation is simple and straightforward, it requires large computational resources to carry out simulations for a long period (typically a few tens of thousand time steps for a few tens of femtosecond). Therefore, it is desirable to find representations which require less computational resources without harming accuracy of the results. In this paper, we consider basis expansion methods converting the 3D grid representation into dense matrix representations of smaller dimensions. We will consider a few choices of basis functions and examine their performances.

To convert the 3D grid representation into a dense matrix representation, a simple and natural choice may be to adopt a finite set of eigenstates of the static Hamiltonian as a basis set to express the time-dependent orbital wave functions. For each  $k$ -point, we prepare occupied and unoccupied orbitals by solving,

$$h[\vec{k}]v_{n\vec{k}}(\vec{r}) = \epsilon_{n\vec{k}}v_{n\vec{k}}(\vec{r}). \quad (3)$$

We then expand the Bloch orbitals  $u_{n\vec{k}}(\vec{r}, t)$  in terms of the eigenfunctions  $v_{m\vec{k}}(\vec{r})$ ,

$$u_{n\vec{k}}(\vec{r}, t) = \sum_m c_m^{n\vec{k}}(t)v_{m\vec{k}}(\vec{r}), \quad (4)$$

where  $c_m^{n\vec{k}}(t)$  is a time-dependent coefficient for the expansion. We call it the  $k$ -fixed basis expansion. If we includes all eigenfunctions in the expansion, it gives the same result as that in the 3D grid representation, since they constitute a complete set. Truncating the unoccupied orbitals, we obtain an approximate matrix equation for the coefficients  $\{c_m^{n\vec{k}}(t)\}$ . However, as will be shown later, the convergence with respect to the number of unoccupied orbitals is very slow for some observables such as the current induced by the optical electric field, which in turn results in the slow convergence for the real part of the dielectric function.

As an alternative basis set, Houston states have been extensively investigated and utilized to calculate time evolutions of orbitals [27, 28]. The Houston states are defined as eigensfunctions of the single-electron Hamiltonian  $h[\vec{k} + e\vec{A}(t)/\hbar c]$  at each time. They are

given by

$$v_{m\vec{k}}^H(\vec{r}, t) = v_{m\vec{k}+e\vec{A}(t)/\hbar c}(\vec{r}) \exp \left[ -\frac{i}{\hbar} \int^t dt' \epsilon_{n\vec{k}+e\vec{A}(t')/\hbar c} \right], \quad (5)$$

and are regarded as exact solutions in the adiabatic limit that is the limit of slow variation of the electric field,  $\vec{E}(t)$ . The Houston states have been used to investigate Bloch oscillations, Wannier-Stark ladders, and so on [27–30]. Using the Houston states, we may expand the Bloch orbitals as follows,

$$u_{n\vec{k}}(\vec{r}, t) = \sum_m c_m^{n\vec{k}}(t) v_{m\vec{k}}^H(\vec{r}, t). \quad (6)$$

We may expect a fast convergence of the calculation for processes in which adiabatic approximation is well satisfied.

In practice, however, there are difficulties in preparing the Houston states in the first-principles descriptions. For example, consider a case when two orbitals, one occupied and the other unoccupied, are (almost) degenerate at a certain  $k$ -point. When the crystalline momentum with a shift of vector potential,  $\vec{k} + e\vec{A}(t)/\hbar c$ , goes through the crossing point, it is difficult to decide which orbital should be occupied beyond the point. Because of the difficulty, we will not explore the expansion using the Houston states. Instead we will consider an alternative expansion which effectively takes account of important aspects of the Houston states.

The essence of the expansion using the Houston states is a use of orbitals with crystalline momentum shifted by the external field. This indicates that we should incorporate orbitals of shifted  $k$ -points in the basis functions, in addition to the orbitals of the original  $k$ -point. Of course, a set of all occupied and unoccupied orbitals for any  $k$ -points spans a complete set. Therefore, any orbitals of a different  $k$ -point may eventually be expressible using eigenfunctions of the original  $k$ -point. However, inclusion of  $k$ -shifted orbitals remarkably accelerates the convergence of the expansion, as will be shown later.

Our prescription to use the orbitals with different  $k$ -points is summarized as follows. To express time-dependent Bloch orbitals  $u_{n\vec{k}}(\vec{r}, t)$ , we employ occupied orbitals of the Hamiltonian in which crystalline momenta are shifted from the original  $k$ -point,  $\vec{k} + e\Delta\vec{A}/\hbar c$ , in addition to occupied and unoccupied orbitals of the original  $k$ -point. We call it the  $k$ -shifted basis expansion. We expect the Houston states  $v_{n\vec{k}}^H(\vec{r}, t)$  may be described well by a superposition of orbitals of the original  $k$ -point,  $v_{n\vec{k}}(\vec{r})$ , and those of shifted  $k$ -points,  $v_{n\vec{k}+e\Delta\vec{A}/\hbar c}(\vec{r})$ . We note that orbitals of different  $k$ -points are no more orthogonal to each other. In our

practical calculations, we first prepare an orthonormalized basis set from orbitals of different  $k$ -points.

In the following section, we will examine performance of the  $k$ -shifted basis expansion for electron dynamics calculations. For comparison, we will compare results of  $k$ -shifted basis expansion with those of  $k$ -fixed basis expansion, and with those without any basis expansions, namely, direct calculations in the 3D grid representation.

### III. LINEAR RESPONSE

To test the basis expansion methods, we calculate a dielectric function of  $\alpha$ -quartz using a density functional Hamiltonian. We calculate the dielectric function from a real time evolution of orbitals employing  $k$ -fixed and  $k$ -shifted basis expansions as well as 3D grid representation without any basis expansions. We note that responses to any weak external fields are fully characterized by the dielectric function.

We use a first-principles density functional Hamiltonian in the local density approximation (LDA) [31]. We denote the static Kohn-Sham Hamiltonian as

$$h_{KS} = \frac{p^2}{2m} + V_{loc} + V_{nonloc}, \quad (7)$$

where  $V_{loc}$  is a local potential composed of electron-ion and electron-electron interactions.  $V_{nonloc}$  is a nonlocal electron-ion interaction in the pseudopotential description [32] with a separable approximation [33]. We ignore local field effects which may be included in the TDDFT. We have confirmed that the local field effects are very small in the TDDFT under the adiabatic LDA. It is well-known that the dielectric functions in the LDA are not accurate enough to reproduce measured features. However, since our purpose here is to compare efficiencies of different numerical methods, we consider it is sufficient.

The time evolution of Bloch orbitals is described by

$$i\hbar \frac{\partial}{\partial t} u_{nk}(r, t) = \left[ \frac{1}{2m} \left( \vec{p} + \hbar \vec{k} + \frac{e}{c} \vec{A}(t) \right)^2 + V_{loc} + e^{-i(\hbar \vec{k} + e \vec{A}(t)/c) \cdot \vec{r}} \hat{V}_{nonloc} e^{i(\hbar \vec{k} + e \vec{A}(t)/c) \cdot \vec{r}} \right] u_{nk}(r, t), \quad (8)$$

where  $\vec{A}(t)$  is a vector potential which is related to the applied electric field  $\vec{E}(t)$  by  $\vec{E}(t) = -\frac{1}{c} \frac{d\vec{A}(t)}{dt}$ . Optical properties can be extracted from the current averaged over the unit cell,

which is induced by the applied electric field,

$$\vec{J}(t) = -\frac{e}{\Omega} \sum_{n, \vec{k}} \int_{\Omega} d\vec{r} d\vec{r}' u_{n\vec{k}}^*(\vec{r}, t) e^{-i(\vec{k}+e\vec{A}(t)/\hbar c) \cdot \vec{r}} \vec{v}(\vec{r}, \vec{r}') e^{i(\vec{k}+e\vec{A}(t)/\hbar c) \cdot \vec{r}'} u_{n\vec{k}}(\vec{r}', t), \quad (9)$$

where  $\Omega$  is the volume of the unit cell and the velocity operator  $\vec{v}(\vec{r}, \vec{r}')$  is defined by

$$\vec{v}(\vec{r}, \vec{r}') = \frac{-i\hbar}{m} \vec{\nabla} \delta(\vec{r} - \vec{r}') + \frac{1}{i\hbar} [\vec{r} \hat{V}_{nonloc}(\vec{r}, \vec{r}') - \hat{V}_{nonloc}(\vec{r}, \vec{r}') \vec{r}']. \quad (10)$$

For a weak field, the applied electric field and the induced current are linearly related by the conductivity. Assuming the field has only a  $\beta$ -direction component, the frequency-dependent conductivity  $\sigma_{\alpha\beta}(\omega)$  and the dielectric function  $\epsilon_{\alpha\beta}(\omega)$  are given as follows:

$$\sigma_{\alpha\beta}(\omega) = \frac{\int_{-\infty}^{\infty} dt e^{i\omega t} J_{\alpha}(t)}{\int_{-\infty}^{\infty} dt e^{i\omega t} E_{\beta}(t)}, \quad \epsilon_{\alpha\beta}(\omega) = \delta_{\alpha\beta} + \frac{4\pi i \sigma_{\alpha\beta}(\omega)}{\omega}. \quad (11)$$

For any choices of the electric field,  $E_{\beta}(t)$ , we may obtain the same results for the conductivity and the dielectric function so long as the field used in the calculation is sufficiently weak. For computational convenience, we employ an impulsive electric field,  $E_{\beta}(t) = d\delta(t)$ , where  $d$  is a parameter specifying the intensity of the field. This choice is equivalent to a constant shift of the vector potential,  $A_{\beta}(t) = -cd\theta(t)$ . Using the impulsive field, the conductivity as a function of time,  $\sigma_{\alpha\beta}(t)$ , is proportional to the induced current,  $J_{\alpha}(t)$ . To reduce numerical noises which originate from a finite period of the calculation, we introduce a mask function in the Fourier transformation,

$$\sigma_{\alpha\beta}(\omega) = \frac{1}{d} \int_0^T dt e^{i\omega t} J_{\alpha}(t) W(t/T), \quad (12)$$

where  $T$  is the period of the time evolution. For the mask function  $W(x)$ , we employ  $W(x) = 1 - 3x^2 + 2x^3$ .

For the calculations of SiO<sub>2</sub>, we choose a unit cell of rectangular parallelepiped containing six silicon and twelve oxygen atoms, 96 valence electrons in total. We note that the number of occupied orbitals at each  $k$ -point is 48 since all orbitals are doubly occupied. We first calculate the ground state using a uniform grid representation in the 3D Cartesian coordinates. We choose  $z$ -axis parallel to the  $c$ -axis of the  $\alpha$ -quartz, and discretize the  $x$ ,  $y$ , and  $z$  coordinates of the unit cell into 20, 36 and 50 grid points, respectively. For the Brillouin zone, we sample it using  $4 \times 4 \times 4$  grid points. Using the 3D grid representation, we can directly calculate the time propagation of the orbitals using, for example, the Taylor

expansion method [34, 35]. We will call it the 3D grid calculation. We also use the 3D grid representation to calculate occupied and unoccupied orbitals in the ground state by solving Eq. (3). These orbitals will be used in the  $k$ -fixed and  $k$ -shifted basis expansions. We use the Taylor expansion method for all time-propagation calculations of  $k$ -fixed,  $k$ -shifted basis expansions as well as 3D grid calculations.

### A. $k$ -fixed basis expansion

We first examine the  $k$ -fixed basis expansion described by Eq. (4). Figure 1 shows the real part of the dielectric function of  $\alpha$ -quartz using  $k$ -fixed basis expansions with various truncations of unoccupied orbitals as well as that in the 3D grid calculation. In the figure,  $k$ -fixed basis expansions are denoted as  $k$ -fixed ( $N_{unocc}$ ), where  $N_{unocc}$  is the number of unoccupied orbitals employed in the expansion at each  $k$ -point. For example,  $k$ -fixed (464) means employment of 48 occupied and 464 unoccupied orbitals. We note that, in the calculation of 48 occupied and 464 unoccupied orbitals, the matrix dimension of the Hamiltonian is 512. This is much smaller than the dimension in the 3D grid representation which is equal to the number of the grid points,  $20 \times 36 \times 50 = 36000$ .

In the figure, one can find that the real part of the dielectric function using the  $k$ -fixed basis expansion shows negative divergent behavior which is absent in the 3D grid calculation. The divergent behavior diminishes as the number of unoccupied orbitals employed in the expansion increases. However, the convergence is rather slow. Even when the  $k$ -fixed basis expansion includes 512 orbitals in total, the dielectric function in the  $k$ -fixed basis expansion is much different from that of the 3D grid calculation.

Figure 2 (a) shows the imaginary part of the dielectric function below 20 eV, while Figure 2 (b) shows that above 20 eV. The imaginary part below 20 eV is well described by the  $k$ -fixed basis expansion with any number of unoccupied orbitals, except below 2 eV. The  $k$ -fixed basis expansion calculation brings unphysical oscillations below 2 eV, which are absent in the 3D grid calculation. This oscillation is sensitive to the number of unoccupied orbitals used in the  $k$ -fixed basis expansion and diminishes with increasing the number of unoccupied orbitals. We next look at responses at higher energy. As seen from the panel (b), the result of the  $k$ -fixed basis expansion becomes poor as the excitation energy increases. This can be explained by the truncation of the basis functions. The energy difference between



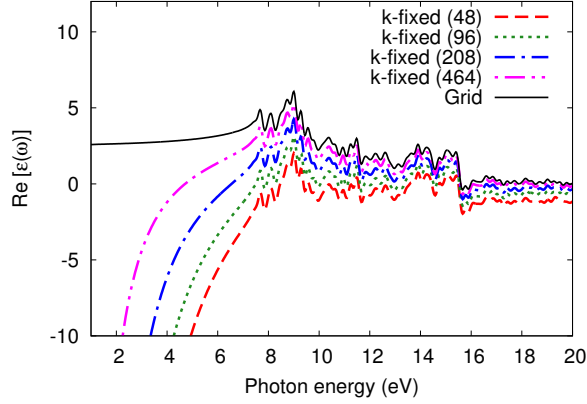


FIG. 1. Real part of the dielectric function of  $\alpha$ -quartz calculated by using several  $k$ -fixed basis expansions. The number in the parenthesis of the legends represents the number of unoccupied orbitals employed at each  $k$ -point. Black-solid line shows results of the 3D grid calculation.

the highest occupied orbital and the highest unoccupied orbital in the truncations is given approximately by 19 eV for the  $k$ -fixed (48), 31 eV for the  $k$ -fixed (96), 51 eV for the  $k$ -fixed (208), and 92 eV for the  $k$ -fixed (464) basis expansions. In Fig. 2 (b), one can find a deviation between the 3D grid calculation and the  $k$ -fixed basis expansions starts to occur at the corresponding energies. For example, results of the  $k$ -fixed (48) basis expansion and of the 3D grid calculation differ much above 21 eV, which roughly coincides with the energy difference of 19 eV between the highest occupied orbitals and the highest unoccupied orbitals included in the  $k$ -fixed (48) basis expansion.

## B. $k$ -shifted basis expansion

We next examine the  $k$ -shifted basis expansion, adding occupied orbitals of nearby  $k$ -points to the basis. Since the magnitude of the vector potential,  $\vec{A}(t)$ , may be infinitesimally small in linear response calculations, we may use a small value for the  $k$ -shifts. In practice, for responses in  $z$ -direction, we employ occupied orbitals at shifted  $k$ -points of  $e\Delta\vec{A}/\hbar c = (0, 0, 0.01)$  and at  $e\Delta\vec{A}/\hbar c = (0, 0, -0.01)$  in atomic unit. We denote the  $k$ -shifted basis expansion as  $k$ -shifted-2 ( $N_{unocc}$ ), where the number 2 indicates that we employ occupied orbitals at two shifted  $k$ -points,  $(0, 0, \pm 0.01)$  in the present case, and  $N_{unocc}$  represents the number of unoccupied orbitals at the original  $k$ -point. For example the  $k$ -shifted-2 (144)

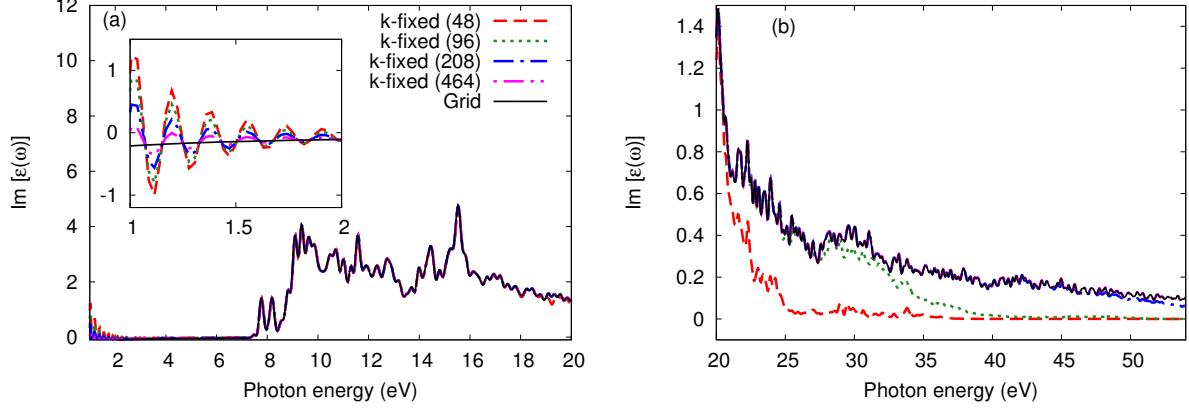


FIG. 2. Imaginary part of dielectric functions of  $\alpha$ -quartz calculated by using several  $k$ -fixed basis expansion. The number in the parenthesis of the legends represents the number of unoccupied orbitals employed at each  $k$ -point. Black-solid line shows results of the 3D grid calculation. The panel (a) shows lower energy region from 1 eV to 20 eV, and the panel (b) shows higher energy region from 20 eV to 54 eV.

basis expansion includes 144 unoccupied orbitals at the original  $k$ -point as well as  $48 \times 3$  occupied orbitals at the original  $k$ -point and two shifted  $k$ -points. Thus, it includes 288 orbitals in total.

Figure 3 shows dielectric function using the  $k$ -shifted basis expansions of different numbers of unoccupied orbitals, and that of the 3D grid calculation. As seen from the figure, the  $k$ -shifted-2 (48) and (144) basis expansions well reproduce both real and imaginary parts of the dielectric function in the 3D grid calculation. Since the real part of the dielectric function cannot be described in the  $k$ -fixed basis expansion as shown in Fig. 1, the present result clearly indicates that the inclusion of the  $k$ -shifted orbitals is essential to describe the linear response accurately.

In Fig. 3, we find the  $k$ -shifted basis expansion without any unoccupied orbitals of original  $k$ -point, the blue-dash-dotted curve of  $k$ -shifted-2 (0), fails to reproduce either real or imaginary parts of the dielectric function. This fact indicates that inclusion of both occupied orbitals of shifted  $k$ -point and unoccupied orbitals of original  $k$ -point are indispensable to correctly describe the linear response.

Although we here calculate the dielectric function using the real time method, the importance of including  $k$ -shifted occupied orbitals in linear response calculations should also

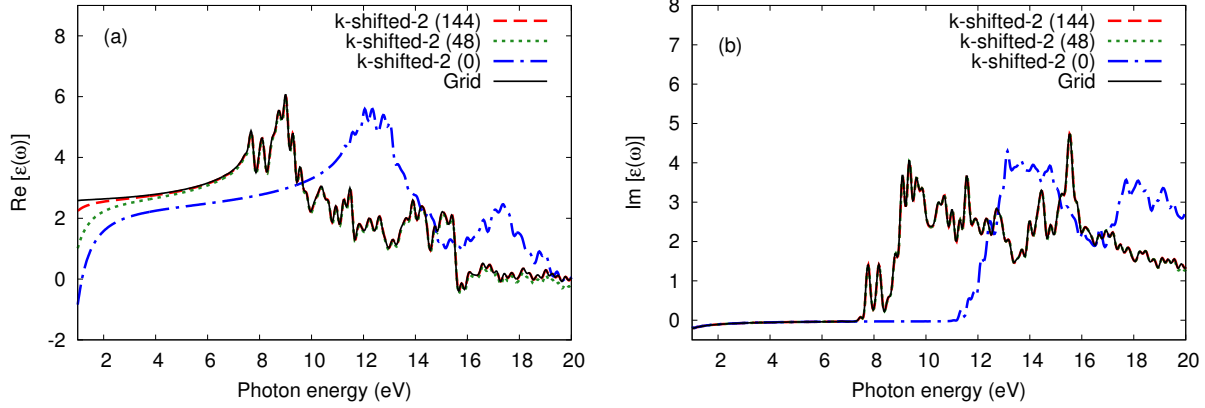


FIG. 3. Real (a) and imaginary (b) parts of the dielectric function of  $\alpha$ -quartz calculated by using  $k$ -shifted basis expansions. The number in the parentheses of legends represents the number of unoccupied orbitals employed at original  $k$ -point. The result of the 3D grid calculation is also shown.

be true in other computational methods such as the Sternheimer method in which linear response for a given frequency is calculated solving linear algebraic equations.

### C. Intra-band and inter-band transitions

In this subsection, we present an analytical investigation on the reason why the inclusion of  $k$ -shifted occupied orbitals brings fast convergence for the calculation of the dielectric function.

We start with the following formal solution of Eq. (8):

$$u_{n\vec{k}}(\vec{r}, t) = \hat{T} \exp \left[ -\frac{i}{\hbar} \int_{t_0}^t dt' h[\vec{k} + e\vec{A}(t')/\hbar c] \right] u_{n\vec{k}}^{GS}(\vec{r}), \quad (13)$$

where  $\hat{T}$  is the time ordering operator. As we described below Eq. (11), we consider an impulsive distortion given by  $\vec{E} = -s\hbar\delta(t)/e$  with  $\vec{s} = s\vec{e}_\beta$ , where  $s$  is an infinitesimally small parameter and  $\vec{e}_\beta$  is a unit vector in  $\beta$  direction. For this distorting field, the Hamiltonian  $h[\vec{k} + e\vec{A}(t)/\hbar c]$  can be described as follows:

$$h[\vec{k} + e\vec{A}(t)/\hbar c] = \frac{1}{2m} (\vec{p} + \hbar\vec{k} + \hbar\vec{s}\Theta(t))^2 + V = \begin{cases} h[\vec{k} + \vec{s}] & (t > 0) \\ h[\vec{k}] & (t \leq 0). \end{cases} \quad (14)$$

The induced current averaged over the unit cell is given by Eq. (9). We decompose the current into orbitals,  $\vec{J}(t) = \sum_{n\vec{k}} \vec{J}_{n\vec{k}}(t)$ . We define a change of the current of each orbital by

$$\begin{aligned} \delta \vec{J}_{n\vec{k}}(t) &= \left( \vec{J}_{n\vec{k}}(t) - \vec{J}_{n\vec{k}}(t=0) \right) \\ &= -\frac{e}{\Omega} \left[ \langle u_{n\vec{k}}^{GS} | e^{i\hbar[\vec{k}+\vec{s}]t/\hbar} e^{-i(\vec{k}+\vec{s})\cdot\vec{r}} \vec{v} e^{i(\vec{k}+\vec{s})\cdot\vec{r}} e^{-i\hbar[\vec{k}+\vec{s}]t/\hbar} | u_{n\vec{k}}^{GS} \rangle - \langle u_{n\vec{k}}^{GS} | e^{-i\vec{k}\cdot\vec{r}} \vec{v} e^{i\vec{k}\cdot\vec{r}} | u_{n\vec{k}}^{GS} \rangle \right]. \end{aligned} \quad (15)$$

Applying the first order perturbation theory to Eq. (15) assuming a small distortion amplitude of  $s$ , the  $\alpha$ -component of the current can be expressed as follows:

$$\begin{aligned} \delta J_{n\vec{k}}^\alpha(t) &= -s \frac{e}{\Omega \hbar} \frac{\partial^2 \epsilon_{n\vec{k}}}{\partial k_\alpha \partial k_\beta} + s \frac{e \hbar}{\Omega} \sum_{n' \neq n} \frac{\langle u_{n\vec{k}}^{GS} | e^{-i\vec{k}\cdot\vec{r}} v^\alpha e^{i\vec{k}\cdot\vec{r}} | u_{n'\vec{k}}^{GS} \rangle \langle u_{n'\vec{k}}^{GS} | e^{-i\vec{k}\cdot\vec{r}} v^\beta e^{i\vec{k}\cdot\vec{r}} | u_{n\vec{k}}^{GS} \rangle}{\epsilon_{n\vec{k}} - \epsilon_{n'\vec{k}}} \\ &\quad \times \left\{ e^{i(\epsilon_{n\vec{k}} - \epsilon_{n'\vec{k}})t/\hbar} + e^{-i(\epsilon_{n\vec{k}} - \epsilon_{n'\vec{k}})t/\hbar} \right\}, \end{aligned} \quad (16)$$

where  $\delta J_{n\vec{k}}^\alpha$  and  $v^\alpha$  represent  $\alpha$ -components of  $\delta \vec{J}_{n\vec{k}}$  and  $\vec{v}$ , respectively. The first term of the right hand side is defined as follows:

$$\frac{\partial^2 \epsilon_{n\vec{k}}}{\partial k_\alpha \partial k_\beta} = \hbar \lim_{s \rightarrow 0} \frac{1}{s} \left[ \langle u_{n\vec{k}+\vec{s}}^{GS} | e^{-i(\vec{k}+\vec{s})\cdot\vec{r}} v^\alpha e^{i(\vec{k}+\vec{s})\cdot\vec{r}} | u_{n\vec{k}+\vec{s}}^{GS} \rangle - \langle u_{n\vec{k}}^{GS} | e^{-i\vec{k}\cdot\vec{r}} v^\alpha e^{i\vec{k}\cdot\vec{r}} | u_{n\vec{k}}^{GS} \rangle \right]. \quad (17)$$

The first term of Eq. (16) is a time-independent current induced by intra-band transitions. The second term is a time-dependent oscillating current induced by inter-band transitions. We thus call the first and the second terms intra-band and inter-band currents, respectively.

Applying the Fourier analysis of Eq. (11) to the current of Eq. (15), one can obtain an analytic form of the dielectric function as follows:

$$\epsilon_{\alpha\beta}(\omega) = 1 + \frac{4\pi i}{\omega} \sum_{n\vec{k}} \sigma_{\alpha\beta}^{n\vec{k}}, \quad (18)$$

where  $\sigma_{\alpha\beta}^{n\vec{k}}$  is a conductivity decomposed into orbitals and  $k$ -points. They are given by

$$\begin{aligned} \sigma_{\alpha\beta}^{n\vec{k}}(\omega) &= i \frac{e^2}{\Omega \hbar^2} \frac{\partial^2 \epsilon_{n\vec{k}}}{\partial k_\alpha \partial k_\beta} \frac{1}{\omega + i\gamma} - i \frac{e^2}{\Omega} \sum_{n' \neq n} \frac{\langle u_{n\vec{k}}^{GS} | e^{-i\vec{k}\cdot\vec{r}} v^\alpha e^{i\vec{k}\cdot\vec{r}} | u_{n'\vec{k}}^{GS} \rangle \langle u_{n'\vec{k}}^{GS} | e^{-i\vec{k}\cdot\vec{r}} v^\beta e^{i\vec{k}\cdot\vec{r}} | u_{n\vec{k}}^{GS} \rangle}{\epsilon_{n'\vec{k}} - \epsilon_{n\vec{k}}} \\ &\quad \times \left[ \frac{1}{\epsilon_{n'\vec{k}} - \epsilon_{n\vec{k}} - \omega - i\gamma} + \frac{1}{\epsilon_{n\vec{k}} - \epsilon_{n'\vec{k}} - \omega - i\gamma} \right]. \end{aligned} \quad (19)$$

Here we added a small imaginary quantity  $\gamma$  in the frequency. We note that the second derivative of the single particle energy is proportional to the inverse of the effective mass of electrons  $\partial^2 \epsilon_{n\vec{k}} / \partial k_\alpha \partial k_\beta = \hbar^2 / m_{\alpha\beta}^*$ . In Eq. (19), the intra-band transitions contribute to the

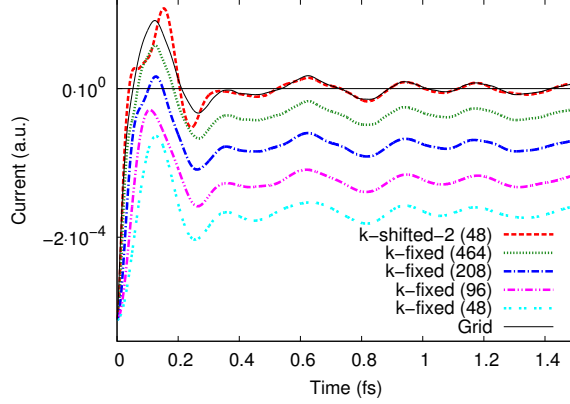


FIG. 4. Currents as functions of time induced by an instantaneous distortion at  $t = 0$ . Results of  $k$ -fixed basis expansions,  $k$ -shifted basis expansion, and the 3D grid calculation are shown.

first term which shows a Drude behavior, and the inter-band transitions contributes to the second term.

For insulators, the first Drude term of Eq. (19) should be identically zero after integrating it over  $k$ . In the  $k$ -fixed basis expansion, however, we found a Drude-like contribution in the real part of the dielectric function as seen in Fig.1. This indicates that the slow convergence in the  $k$ -fixed basis expansion comes from a failure to cancel the intra-band transitions which should vanish if one includes all unoccupied orbitals.

Figure 4 shows electric currents as functions of time after the distortion is applied at  $t = 0$ . The currents using the  $k$ -fixed basis expansion, the  $k$ -shifted basis expansion, and the 3D grid calculation are shown. These currents are used in the calculations of dielectric functions shown in Fig 1, 2, and 3.

As expected, one sees that large constant components appear in the currents of the  $k$ -fixed basis expansions. As the number of unoccupied orbitals increases in the  $k$ -fixed basis expansion, the constant component of the current decreases. However, the constant component remains substantial even when a large number of unoccupied orbitals, 464 orbitals, is employed in the  $k$ -fixed (464) basis expansion. In contrast, the current of the  $k$ -shifted basis expansion oscillates around zero-value without any constant components and coincides well with the result of the 3D grid calculation.

Summarizing the findings in this subsection, the  $k$ -fixed basis expansion fails to describe the current caused by the intra-band transitions which should vanish in any insulators.

Since the appearance of the constant current in the  $k$ -fixed basis expansion indicates that the fundamental property of insulators cannot be described adequately, the  $k$ -fixed basis expansion should not be used for the electron dynamics calculations. We have found the addition of the occupied orbitals of shifted  $k$ -points to the basis functions of original  $k$ -point solves the problem. The  $k$ -shifted basis expansion efficiently describes the electron dynamics in insulators in the linear response regime.

#### IV. ELECTRON DYNAMICS INDUCED BY PULSED ELECTRIC FIELDS

In this section, we examine usefulness of the  $k$ -shifted basis expansion to describe electron dynamics under pulsed electric fields. In the following calculations, we employ the pulsed electric field described by the vector potential,

$$\vec{A}(t) = \vec{e}_z \frac{cE_0}{\omega} \cos(\omega t) \sin^2\left(\frac{\pi t}{T_p}\right) \quad (0 < t < T_p), \quad (20)$$

where  $\omega$  represents the mean frequency of the pulse field for which we take  $\omega = 3.10$  eV/ $\hbar$ , and  $T_p$  represents a pulse duration for which we take  $T_p = 10.67$  fs corresponding to eight cycles. We define the peak laser intensity of the pulsed electric field by  $I = cE_0^2/8\pi$ . We will consider electron dynamics in  $\alpha$ -quartz as before, for two cases of different field intensities.

We calculate two physical quantities to examine quality of the representations. One is the electric current,  $\vec{J}(t)$ , defined by Eq. (9). The other is the electronic excitation energy of the system per unit cell,  $E_{ex}(t)$ , defined as follows:

$$E_{ex}(t) = \sum_{n\vec{k}} \int_{\Omega} d\vec{r} u_{n\vec{k}}^*(\vec{r}, t) \hbar \left[ \vec{k} + \frac{e}{\hbar c} \vec{A}(t) \right] u_{n\vec{k}}(\vec{r}, t) - E_{GS}, \quad (21)$$

where  $E_{GS}$  is the energy of the ground state.

##### A. Electron dynamics under a weak pulsed electric field

First we examine basis expansion methods applied for electron dynamics under a weak pulsed electric field. The peak laser intensity is set to  $I = 1.0 \times 10^{10}$  W/cm<sup>2</sup>. At this intensity, electron dynamics is well described by the linear response theory. Since the frequency  $\omega = 3.10$  eV/ $\hbar$  is below the optical band gap of  $\alpha$ -quartz which is 6.3 eV in the present LDA calculation, real electronic excitations do not take place.

We show results using  $k$ -fixed basis expansions in Fig. 5. Figure 5 (a) shows currents and (b) shows excitation energies per unit cell as functions of time. The black-solid lines represent results of the 3D grid calculation, while other lines show results of  $k$ -fixed basis expansions. The number of unoccupied orbitals employed is denoted in the parentheses.

As seen from the panel (a), calculations using  $k$ -fixed basis expansions cannot reproduce the current of the 3D grid calculation. Even the sign of the current is opposite between the  $k$ -fixed basis expansions and the 3D grid calculation. The magnitude of the current in the  $k$ -fixed basis expansion is much larger than that in the 3D grid calculation, even using the largest number of unoccupied orbitals,  $k$ -fixed (464). These observations are consistent with the dielectric function calculated using the  $k$ -fixed basis expansions. Namely, in Fig. 1, the real part of the dielectric function is negative at the frequency of,  $\hbar\omega = 3.1$  eV, in the  $k$ -fixed basis expansions, which is opposite in sign to the 3D grid calculation. The magnitude of the dielectric function decreases as the number of unoccupied basis functions increases.

In the panel (b), one can find that the excitation energy during the pulse field irradiation is always overestimated in the  $k$ -fixed basis expansions. The times when excitation energy shows maximum are different between the 3D grid calculation and the  $k$ -fixed basis expansion. The energy maximum of the 3D grid calculation takes place when the magnitude of the electric field is maximum, while the energy maximum in the  $k$ -fixed basis expansions takes place when the magnitude of the vector potential shows maximum. These facts indicate that calculations in the  $k$ -fixed basis expansions fail to reproduce the 3D grid calculation even in a qualitative level.

Figure 6 (a) and (b) show currents and excitation energies in the unit cell using the  $k$ -shifted basis expansion. For comparison, results of the 3D grid calculation and of the  $k$ -fixed basis function with the largest number of unoccupied orbitals are shown.

As in the linear response calculation shown in the previous section, we employ occupied orbitals of shifted crystalline momenta,  $e\Delta A/\hbar c = \pm 0.01$ . This value is comparable to the maximum value of the vector potential in Eq. (20) in the present calculation,  $A(t)/\hbar c = 0.0047$  a.u., at  $t = 5.33$  fs.

As seen from both panels (a) and (b) of Fig. 6, calculations using  $k$ -shifted basis expansion well reproduce results of the 3D grid calculation. Although much more orbitals are used, results in the  $k$ -fixed basis expansion are qualitatively wrong. They are consistent with those in the linear response calculations where, as shown in Fig. 3, the real part of the dielectric

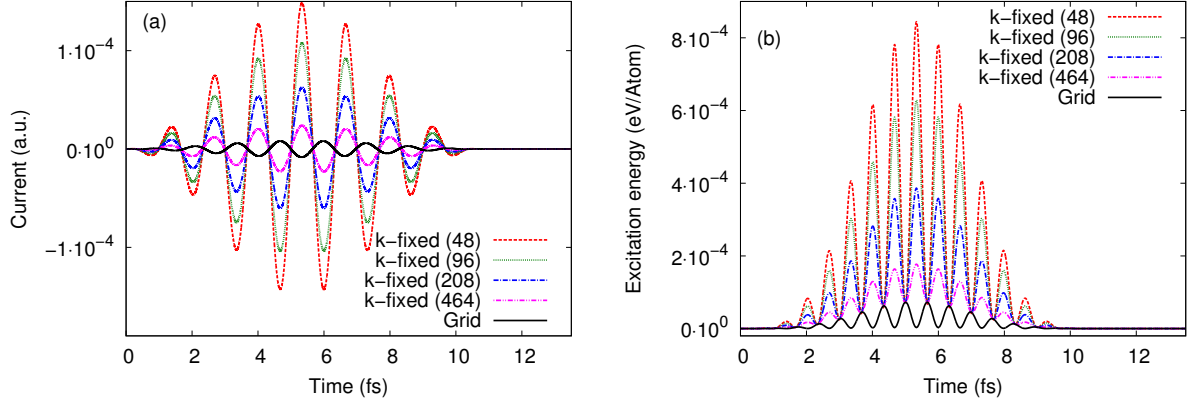


FIG. 5. Currents (a) and excitation energy per unit cell (b) as functions of time are shown. Black-solid line shows results of the 3D grid calculation, while other lines show results of the  $k$ -fixed basis expansions with different truncations. The maximum intensity of the pulsed electric field is set to  $I = 1.0 \times 10^{10} \text{ W/cm}^2$

function at  $\hbar\omega = 3.10 \text{ eV}$  is well described in the  $k$ -shifted basis expansion.

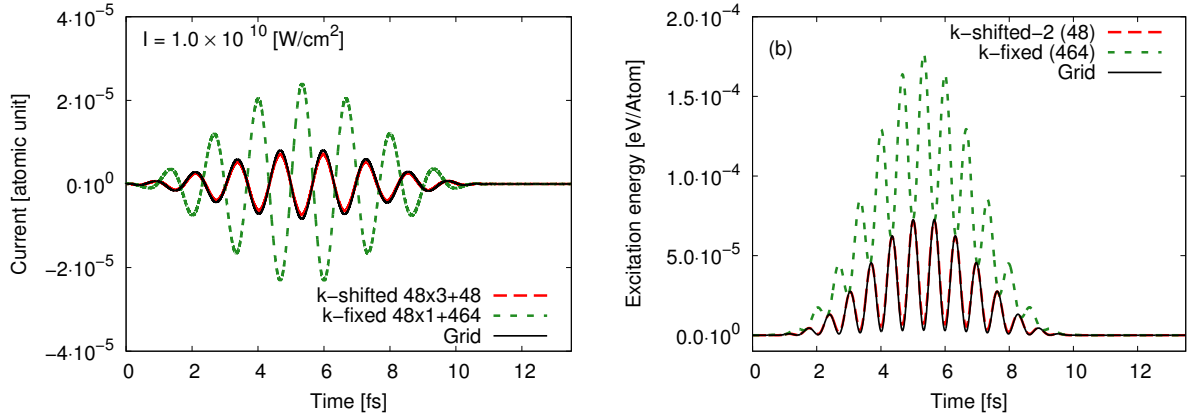


FIG. 6. Currents (a) and excitation energies per unit cell (b) as functions of time are shown. Black-solid line shows results of the 3D grid calculation, red-dashed line shows results of the  $k$ -shifted basis expansion, and green-dotted line shows results of the  $k$ -fixed basis expansion. The maximum intensity of the pulsed electric field is set to  $I = 1.0 \times 10^{10} \text{ W/cm}^2$



## B. Electron dynamics under a strong pulsed electric field

We next move to the case of electron dynamics in  $\alpha$ -quartz under a strong pulsed electric field. The maximum intensity of the pulsed electric field is set to  $5 \times 10^{12}$  W/cm<sup>2</sup>. For this electric field, the maximum absolute value of the vector potential of Eq. (20) reaches  $eA(t)/\hbar c = 0.1$  a.u. at  $t = 5.33$  fs.

We examine two kinds of  $k$ -shifted basis expansions. One is the same as those employed in the linear response calculations of previous subsection,  $k$ -shifted-2 ( $N_{unocc}$ ), in which two shifted  $k$ -points of  $e\Delta A/\hbar c = (0, 0, \pm 0.01)$  are used. The other is  $k$ -shifted-4 ( $N_{unocc}$ ) in which four shifted  $k$ -points of  $e\Delta A/\hbar c = (0, 0, \pm 0.01)$  and  $(0, 0, \pm 0.15)$  are used. We note that the shift of the crystalline momentum 0.15 a.u. is similar in magnitude to the maximum value of the vector potential, 0.1 a.u.

Figure 7 shows electric currents and excitation energies calculated using  $k$ -shifted-2 (48) basis expansion,  $k$ -shifted-2 (144) basis expansion, and  $k$ -shifted-4 (48) basis expansion. For comparison, results in the 3D grid calculation are also shown. We note that the total number of the basis functions is 192 for  $k$ -shifted-2 (48), and 288 for both  $k$ -shifted-2 (144) and  $k$ -shifted-4 (48). At first glance, three calculations of  $k$ -shifted-2 (48),  $k$ -shifted-2 (144), and  $k$ -shifted-4 (48) work reasonably. However, a closer look indicates that the  $k$ -shifted-2 (48) basis expansion, which was successful for the weak pulse case, is not accurate enough. The maximum value of the current is not well reproduced, as seen from (a). In contrast, the  $k$ -shifted-4 (48) and the  $k$ -shifted-2 (144) basis expansions well reproduce the results of the 3D grid calculation. The  $k$ -shifted-4 (48) basis expansion provides slightly better description compared with the  $k$ -shifted-2 (144) basis expansion.

We show one more case using a pulsed electric field whose frequency is lower than, but the maximum value of the vector potential is the same as that used in Fig. 7. The maximum intensity and the mean frequency of the pulsed electric field are set to  $1.25 \times 10^{12}$  W/cm<sup>2</sup> and 1.55 eV/ $\hbar$ , respectively.

Figure 8 shows the currents and the excitation energies as functions of time using basis functions of  $k$ -shifted-4 (48) and  $k$ -shifted-2 (144). The figure shows that results of the  $k$ -shifted-4 (48) basis expansion show better agreement with the 3D grid calculation than those of the  $k$ -shifted-2 (144) basis expansion. This fact indicates that basis functions which include occupied orbitals of more  $k$ -shifted points are required for electron dynamics induced

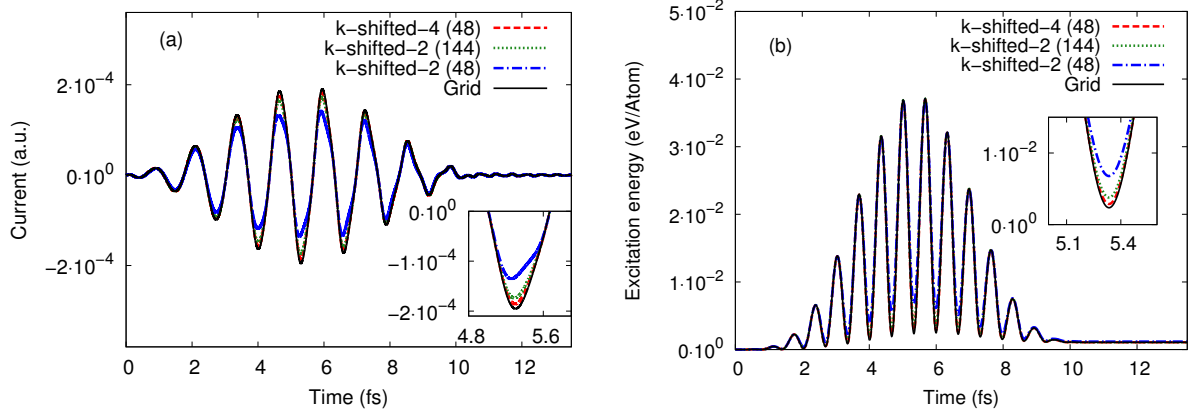


FIG. 7. Currents (a) and excitation energies per unit cell (b) as functions of time are shown. Black-solid line shows results of the 3D grid calculation, while other lines show results of the  $k$ -shifted basis expansions. The maximum intensity of the pulsed electric field is set to  $I = 5.0 \times 10^{12}$  W/cm<sup>2</sup>.

by pulsed electric field of lower frequencies.

## V. COMPUTATIONAL ASPECTS

In this section, we discuss computational speed up of the electron dynamics calculation using the basis expansion method. Here we compare the computational time of  $k$ -shifted-4 (48) basis expansion with that of the 3D grid representation in  $\alpha$ -quartz calculations. We note that the number of basis functions and the number of grid points required to describe accurately the electron dynamics depend on the material and on the choice of the parameters of pulsed electric fields.

There are two aspects in the basis expansion calculations that contribute to speed up the electron dynamics calculations. One is the reduction of the matrix dimension. In 3D grid calculations, the operation of the Hamiltonian on orbitals is an operation of a large-sparse matrix on a vector, while in the  $k$ -shifted basis expansion, a dense matrix operates on a vector. In the present  $\alpha$ -quartz case, the 3D grid calculations employ  $36,000 = 20 \times 36 \times 50$  grid points to describe the Bloch orbitals. This means that the Hamiltonian is a  $36,000 \times 36,000$  sparse matrix. This is reduced to a  $288 \times 288$  dense matrix in the  $k$ -shifted-4 (48) basis expansion. The other is a possible use of longer stride of time in the real-time

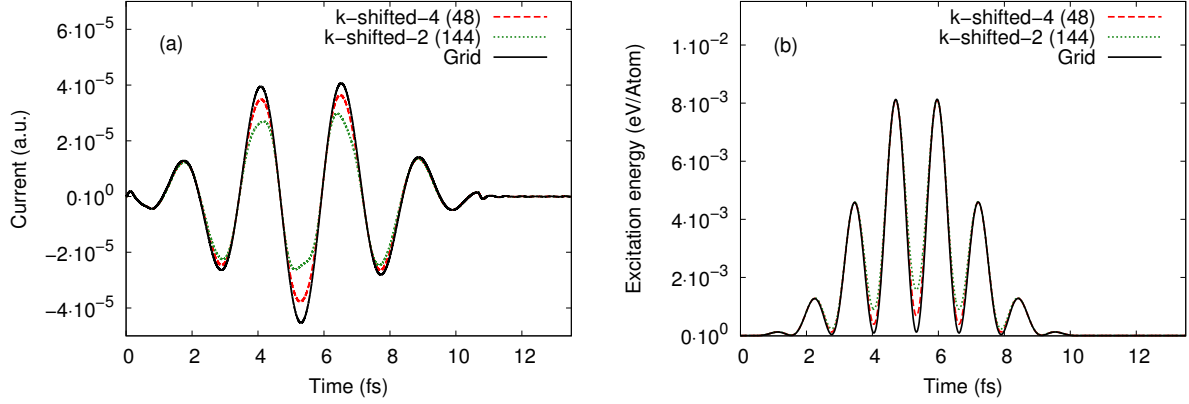


FIG. 8. Currents (a) and excitation energies per unit cell (b) as functions of time are shown. Black-solid line shows results of the 3D grid calculation, red-dashed line shows results of the  $k$ -shifted-4 (48) basis expansion, and green-dotted line shows results of the  $k$ -shifted-2 (144) basis expansion. The maximum intensity and the mean frequency of the pulsed electric field is set to  $I = 1.25 \times 10^{12} \text{W/cm}^2$  and  $\omega = 1.55 \text{eV}/\hbar$ , respectively.

evolution. In explicit methods such as the Taylor expansion method which we usually adopt in the 3D grid representation, the stride which provides stable time evolution is limited by the maximum eigenvalue of the Hamiltonian. In the 3D grid representation, the maximum eigenvalue may be estimated from the grid spacing  $\Delta x$  by  $E_{max} = 3\hbar^2(\pi/\Delta x)^2/2m$ . The maximum eigenvalue in the orbital expansion methods is much smaller than that of 3D grid representation.

We first investigate the speed up coming from the reduction of the matrix dimension. We compare the computational time of the real-time evolution, employing the same stride of time step,  $\Delta t = 0.02$  a.u. and the number of time steps,  $N_t = 28,000$ . This time step is appropriate in the 3D grid representation. We confirmed that the time evolution calculation is not stable if we use a larger step,  $\Delta t = 0.03$  a.u., in the 3D grid representation. The time evolution calculation is carried out at the T2K-Tsukuba supercomputer, University of Tsukuba. We employed 64 CPU cores to parallelize the calculation distributing different  $k$ -points,  $64 = 4 \times 4 \times 4$   $k$ -points, into cores. We have found that the calculation in the 3D grid representation costs 16.71 hours, while the calculation in the  $k$ -shifted-4 (48) basis expansion costs 1.05 hours. Therefore the speed up by reducing the matrix dimension is about 15 times.

We note that the reduction of the computational time is not simply related to the dimension of the matrix. Since the matrix is sparse in the 3D grid representation while it is dense in the basis expansions, the computational time is much smaller for the sparse matrix if the matrix dimensions are the same.

We next investigate the possibility of employing longer stride for the time step. For the  $k$ -shifted-4 (48) basis expansion calculation, we have found that we may use  $\Delta t = 0.07$  a.u., while the calculation employing  $\Delta t = 0.08$  a.u. results in divergence after a short evolution. Therefore, we can use about 3.5 times longer stride of time in the  $k$ -shifted basis expansion than that in the 3D grid representation. Combining the two speed up factors,  $15 \times 3.5$ , we can speed up about 50 times in the  $k$ -shifted basis expansion compared with the 3D grid calculation.

## VI. SUMMARY AND CONCLUSION

In this paper, we explored efficient basis expansion methods to describe electron dynamics in crystalline solids under an intense and ultrashort laser pulse irradiation as well as under a weak field in the linear response. We utilize a realistic Hamiltonian constructed by the first-principles density functional theory. Employing uniform grid representation in the three-dimensional Cartesian coordinates, we can calculate the evolution of orbitals robustly. However, it costs excessive computational costs.

One may expect that a simple and natural choice for the basis functions would be eigenfunctions of static Kohn-Sham Hamiltonian. However, it turned out that the convergence is very slow with respect to the number of orbitals employed. We then propose to add occupied orbitals of nearby  $k$ -points to the occupied and unoccupied orbitals at original  $k$ -points to mimic the use of Houston functions. We call this procedure the  $k$ -shifted basis expansion. It was found that the  $k$ -shifted basis expansion dramatically improves the description. We demonstrate usefulness of the  $k$ -shifted basis expansion numerically, taking examples of responses of SiO<sub>2</sub> under weak and strong pulsed electric fields. We also clarify analytically the reason why the use of the  $k$ -shifted occupied orbitals improves the description.

We also investigated the computational speed up using the  $k$ -shifted basis expansion. For the electron dynamics calculation of SiO<sub>2</sub>, we found a speed up of about 50 times is achieved employing the  $k$ -shifted basis functions, in comparison with the 3D grid representation. We

expect this method will be much beneficial in the calculations of laser-matter interactions, especially when we couple the dynamics of macroscopic electromagnetism and microscopic electron dynamics.

## ACKNOWLEDGMENTS

This work is supported by the Grants-in-Aid for Scientific Research Nos. 23340113 and 25104702. The numerical calculations were performed on the supercomputer at the Institute of Solid State Physics, University of Tokyo, and T2K-Tsukuba at the Center for Computational Sciences, University of Tsukuba.

- 
- [1] M. D. Perry, B. C. Stuart, P. S. Banks, M. D. Feit, V. Yanovsky, A. M. Rubenchik, *J. Appl. Phys.* **85**, 6803 (1999).
  - [2] T. Brabec, F. Krausz, *Rev. Mod. Phys.* **72**, 545 (2000).
  - [3] A. Couairon and A. Mysyrowicz, *Phys. Rep.* **441**, 47 (2007).
  - [4] E. G. Gamaly, *Phys. Rep.* **508**, 91 (2011).
  - [5] A. V. Mitrofanov, A. J. Verhoef, E. E. Serebyuannikov, J. Lumeau, L. Glebov, A. M. Zheltikov, and A. Baltuska, *Phys. Rev. Lett.* **106**, 147401 (2011).
  - [6] P. Balling and J. Schou, *Rep. Prog. Phys.* **76**, 036502 (2013).
  - [7] M. Schultze, E. M. Bothschafter, A. Sommer, S. Holzner, W. Schweinberger, M. Fiess, M. Hofstetter, R. Kienberger, V. Apalkov, V. S. Yakovlev, M. I. Stockman, and F. Krausz, *Nature* **493**, 75 (2013).
  - [8] A. Schiffrin, T. Paasch-Colberg, N. Karpowicz, V. Apalkov, D. Gerster, S. Mühlbrandt, M. Korbman, J. Reichert, M. Schultze, S. Holzner, J. Barth, R. Kienberger, R. Ernstorfer, V. Yakovlev, M. I. Stockman, and F. Krausz, *Nature* **493**, 70 (2013).
  - [9] E. Runge and E. K. U. Gross, *Phys. Rev. Lett.* **52**, 997 (1984).
  - [10] G. F. Bertsch, J.-I. Iwata, A. Rubio, and K. Yabana, *Phys. Rev. B* **62** 7998 (2000).
  - [11] T. Otobe, M. Yamagiwa, J.-I. Iwata, K. Yabana, T. Nakatsukasa, and G. F. Bertsch, *Phys. Rev. B* **77**, 165104 (2008).

- [12] Y. Shinohara, K. Yabana, Y. Kawashita, J.-I. Iwata, T. Otobe, G. F. Bertsch, Phys. Rev. B **82** 155110 (2010).
- [13] Y. Shinohara, S. A. Sato, K. Yabana, J.-I. Iwata, T. Otobe, G. F. Bertsch J. Chem. Phys. **137**, 22A527 (2012).
- [14] S. A. Sato, K. Yabana, Y. Shinohara, T. Otobe, G. F. Bertsch Phys. Rev. B **89**, 064304 (2014).
- [15] C. Wang, L. Jiang, F. Wang, X. Li, Y.P. Yuan, H.L. Tsai, Phys. Lett. A **375**, 3200 (2011).
- [16] C. Wang, L. Jiang, F. Wang, X. Li, Y.P. Yuan, L.T. Qu, Y.F. Lu, Phys. Lett. A **376**, 3327 (2012).
- [17] C. Wang, L. Jiang, X. Li, F. Wang, Y.P. Yuan, L.T. Qu, Y.F. Lu, J. Appl. Phys. **113**, 143106 (2013).
- [18] V. A. Goncharov, J. Chem. Phys. **139**, 084104 (2013).
- [19] I. Tavernelli, Phys. Rev. B **73**, 094204 (2006).
- [20] L. Plaja and L. Roso-Franco, Phys. Rev. B **45**, 8334 (1992).
- [21] H. Bachau, A. N. Belsky, P. Martin, A. N. Vasil'ev, and B. N. Yatsenko, Phys. Rev. B **74**, 235215 (2006).
- [22] V. Apalkov and M. I. Stockman, Phys. Rev. B **86**, 165118 (2012).
- [23] M. Korbman, S. Yu. Kruchinin and V.S. Yakovlev, New Journal of Physics **15**, 013006 (2013).
- [24] K. Yabana, T. Sugiyama, Y. Shinohara, T. Otobe, G. F. Bertsch, Phys. Rev. B **85** 045134 (2012).
- [25] K.-M. Lee, C. M. Kim, S. A. Sato, T. Otobe, Y. Shinohara, K. Yabana, T.M. Jeong, J. Appl. Phys. **115**, 053519 (2014).
- [26] V. A. Goncharov, K. Varga, Phys. Rev. B **83**, 035118 (2011).
- [27] W. V. Houston, Phys. Rev. **57**, 184 (1940)
- [28] J. B. Krieger and G. J. Iafrate, Phys. Rev. B **33**, 5494 (1986).
- [29] F. Bloch, Z. Phys. **52**, 555 (1929)
- [30] G. H. Wannier, Phys. Rev. **117**, 432 (1960); Rev. Mod. Phys. **34**, 645 (1962)
- [31] J. P. Perdew and A. Zunger, Phys. Rev. B **23**, 5048 (1981).
- [32] N. Troullier and J. L. Martins, Phys. Rev. B **43**, 1993 (1991).
- [33] L. Kleinman and D. M. Bylander, Phys. Rev. Lett. **48**, 1425 (1982).
- [34] K. Yabana and G. F. Bertsch, Phys. Rev. B **54**, 4484 (1996).
- [35] H. Flocard, S. E. Koonin and M. S. Weiss, Phys. Rev. C **17**, 1682 (1978).